D J Med Sci 2026;12(2):69-78
doi: 10.5606/fng.btd.2026.249

Original Article

Synaptic silencing as metabolic self-defense: oxidative stress predicts receptor ratios across the *Caenorhabditis elegans* connectome

Çiğdem Türkmen[1], Barış Topçular[2,3]

[1]*Ci-Tu MedScience, Basel, Switzerland*
[2]*Department of Neurology, Demiroğlu Bilim University, İstanbul, Türkiye*
[3]*FrontoPolar GmbH, Berlin, Germany*

ABSTRACT

Objectives: This study aimed to test, at single-neuron resolution, the central prediction of the synaptic silencing as metabolic self-defense framework — that neurons under greater metabolic pressure preferentially maintain glutamatergic synapses in a functionally silent state, retaining N-methyl-D-aspartate (NMDA) receptors while withdrawing α-amino-3-hydroxy-5-methyl-4-isoxazolepropionic acid (AMPA) receptors — and to determine which component of metabolic state (total bioenergetic load versus oxidative stress) is associated with receptor stoichiometry across the *Caenorhabditis elegans* connectome.

Materials and methods: This retrospective, cross-sectional in silico (computational) study was conducted between January 15th 2026 and June 30th 2026, utilizing integrated multi-omic data from 169 *Caenorhabditis elegans (C. elegans)* neuron classes. We tested predictions of this framework computationally, using single-neuron transcriptomic data from the *Caenorhabditis elegans* Neuronal Gene Expression Map (CeNGEN) integrated with the Witvliet developmental connectome.

Results: To evaluate receptor stoichiometry across 169 neuron classes, we calculated a Silent Synapse Index (SSI) based on the expression ratio of NMDA-type *(nmr-1/nmr-2)* to AMPA-type *(glr-1–glr-8)* receptor transcripts and integrated it with metabolic gene module scores. Oxidative stress defense expression was associated with higher SSI (ρ = 0.201, $p = 0.009$; false discovery rate-adjusted $p = 0.050$), whereas a principal component representing general bioenergetic load was not (ρ = 0.091, $p = 0.24$). At the single-gene level, *xbp-1* expression correlated positively with *glr-1* (ρ = 0.182) and *ire-1* negatively (ρ = −0.205), a divergence consistent with their distinct roles in endoplasmic reticulum export and general stress signaling. A second principal component contrasting unfolded protein response against reactive oxygen species defense expression was also associated with SSI (ρ = −0.163, $p = 0.034$). Effect sizes are modest, and the analysis is correlational.

Conclusion: These findings refine the framework by nominating oxidative stress, rather than total metabolic load, as the candidate bioenergetic signal associated with receptor stoichiometry, and generate specific hypotheses for experimental test.

Keywords: *Caenorhabditis elegans*, connectomics, glutamate receptors, oxidative stress, synaptic silencing.

Synaptic transmission is among the most metabolically expensive operations in the nervous system, with estimates suggesting that synaptic signaling accounts for the majority of neuronal energy expenditure.[1,2] The synaptic silencing as metabolic self-defense framework[3] proposes that neurons can adaptively reduce this cost by maintaining glutamatergic synapses in a functionally silent state, retaining N-methyl-D-aspartate receptors (NMDARs) while withdrawing or inactivating α-amino-3-hydroxy-5-methyl-4-isoxazolepropionic acid receptors (AMPARs). This configuration preserves the structural synapse and its capacity for reactivation while eliminating the energetic cost of basal synaptic transmission, since AMPARs mediate fast excitatory transmission at resting membrane potentials, whereas NMDARs remain voltage-gated by the Mg2+ block.[4]

The framework generates several testable predictions: (1) neurons under greater metabolic

Received: July 17, 2026
Accepted: August 13, 2026
Published online: August 31, 2026

Correspondence: Barış Topçular, MD.
E-mail: baris.topcular@demiroglu.bilim.edu.tr

Cite this article as:
Türkmen Ç, Topçular B. Synaptic silencing as metabolic self-defense: oxidative stress predicts receptor ratios across the *Caenorhabditis elegans* connectome. D J Med Sci 2026;12(2):69-78. doi: 10.5606/fng.btd.2026.249.

pressure should show a higher propensity for synaptic silencing; (2) silencing should preferentially target low-information-yield connections; and (3) the molecular machinery controlling AMPAR trafficking should covary with metabolic gene expression at the single-neuron level. Testing these predictions in mammalian systems is complicated by incomplete connectomic data, bulk-tissue transcriptomic averaging, and the difficulty of measuring metabolic state at cellular resolution.[5,6]

Caenorhabditis elegans (C. elegans) offers a uniquely tractable system for addressing these predictions. Its nervous system contains exactly 302 neurons with a fully reconstructed connectome,[7,8] developmental connectomic trajectories across 8 isogenic individuals,[9] and now a complete gene expression atlas at single-neuron-class resolution through the *Caenorhabditis elegans* Neuronal Gene Expression Map and Network (CeNGEN) project.[10] Critically, *C. elegans* possesses conserved glutamatergic signaling machinery: 8 non-NMDA (AMPA/kainate-type) receptor subunits (*glr-1* through *glr-8*) and 2 NMDA-type subunits *(nmr-1, nmr-2)*, with glutamate receptor-1 (GLR-1) trafficking regulated by the same unfolded protein response (UPR) pathway *(ire-1/xbp-1)* that controls AMPAR export from the endoplasmic reticulum (ER) in mammals.[11,12] Non-conducting AMPA receptors, a potential silencing mechanism distinct from receptor withdrawal, have been observed in *C. elegans* but not in mammals,[4] suggesting that synaptic silencing may be an evolutionarily conserved strategy with species-specific implementations. Here, we integrate CeNGEN single-neuron transcriptomics with the Witvliet developmental connectome to test the three core predictions of the synaptic silencing as metabolic self-defense framework at a resolution unattainable in any mammalian system.

MATERIALS AND METHODS

This retrospective, cross-sectional in silico (computational) study was conducted at the Department of Neurology, Demiroğlu Bilim University between January 15th 2026 and June 30th 2026, utilizing integrated multi-omic data from 169 *C. elegans* neuron classes.

Single-cell RNA-sequencing data were obtained from the CeNGEN project[10] via the WormBase-curated AnnData archive.[13]

Silent synapse index (SSI)

Gene expression was aggregated to neuron-class-level pseudobulk profiles by computing mean expression across all cells within each of the 169 neuron classes. The SSI was computed for each neuron class as a normalized contrast between NMDA-type and AMPA-type ionotropic glutamate receptor expression: SSI_contrast = (ΣNMDAR - ΣAMPAR) / (ΣNMDAR + ΣAMPAR + ε) where ΣNMDAR = *nmr-1* + nmr-2 expression, ΣAMPAR = Σ *glr-1* through *glr-8* expression, and ε = 0.01 (pseudocount). SSIcontrast ranges from −1 (exclusively AMPAR) to +1 (exclusively NMDAR). Neuron classes were classified as NMDAR-dominant (SSI > 0.3), AMPAR-dominant (SSI < −0.3), balanced (−0.3 ≤ SSI ≤ 0.3), AMPAR-only (AMPAR expressed, NMDAR absent), NMDAR-only (NMDAR expressed, AMPAR absent), or non-glutamatergic (neither expressed). Receptor specificity across neuron classes was quantified using the tau index.[14]

Metabolic burden index (MBI)

Metabolic burden was computed from six gene modules: mitochondrial electron transport chain (ETC; 26 genes across Complexes I-V), glycolysis (16 genes), tricarboxylic acid (TCA) cycle (10 genes), UPR (6 genes including *ire-1* and *xbp-1*), reactive oxygen species (ROS) defense (11 genes including *sod-1-5*, *ctl-1-3*, and *skn-1*), and autophagy/mitophagy (11 genes including pink-1, *pdr-1*, and *dct-1*). Each module score was computed as the mean of z-scored gene expression across neuron classes.

Connectome integration

The Witvliet connectome edge list was parsed into a directed graph (223 neurons, 3,676 edges). Per-neuron statistics included degree, strength (weighted degree), eigenvector centrality, betweenness centrality, and fractions of stable, variable, and developmental connections. Individual neuron identities were aggregated to the neuron-class level using standard *C. elegans* nomenclature (removing L/R suffixes and numeric indices), yielding 135 connectome-characterized neuron classes.

Merged analysis included 63 neuron classes with complete data across all three modalities (SSI, MBI, connectome).

Statistical analysis

Spearman rank correlations were used for all bivariate associations. Permutation tests (10,000 permutations) confirmed the robustness of primary results. Multiple testing was corrected using Benjamini-Hochberg false discovery rate (FDR). Principal Component Analysis (PCA) was performed on standardized metabolic module scores to deconvolve metabolic relationships and derive orthogonal axes of variance. Kruskal-Wallis tests compared connectomic metrics across receptor classes. All analyses were conducted in Python 3.9 using SciPy 1.13, statsmodels 0.14, scikit-learn 1.4, and NetworkX 3.2.

Code availability

The code used to perform the analyses described in this study is provided as Extended Data 1.

RESULTS

A total of 169 *C. elegans* neuron classes (comprising 100,955 FACS-sorted cells from L4 larvae; median: 328 genes per cell) from the CeNGEN transcriptomic atlas were included in the study. Developmental connectome data were obtained from the supplementary tables of Witvliet et al.,[9] including 3,676 classified connections across 223 neurons with synapse stability classifications: stable (n = 829), variable (n = 1,995), post-embryonic brain integration (n = 554), developmentally dynamic strengthened (n = 278), and developmentally dynamic weakened (n = 20).

The statistical analyses performed to evaluate the relationships among the study variables are summarized in Table 1, including the data structure, statistical tests applied, sample sizes, correlation coefficients, confidence intervals where applicable, and corresponding significance levels.

Glutamate receptor landscape across the *C. elegans* nervous system

All 10 ionotropic glutamate receptor subunits were detected in the CeNGEN dataset (100% coverage). The AMPA-type receptors showed broader expression than NMDA-type: *glr-5* was detected in 139/169 neuron classes, whereas *nmr-1* was detected in only 45 classes, as

Table 1. Statistical tests

Note	Analysis	Data structure	Type of test	Confidence/power
a	Receptor class distribution across neuron classes	Count data, non-normal	Descriptive frequency distribution	n = 169 neuron classes
b	PC1 (general bioenergetic load) *vs.* SSI	Continuous, non-normal	Spearman rank correlation	ρ = 0.091, p = 0.24, n = 169
c	ROS defence module *vs.* SSI	Continuous, non-normal	Spearman rank correlation, BH-FDR corrected	ρ = 0.201 [95% CI: 0.05, 0.34], p = 0.009, p_FDR = 0.050, n = 169
d	TCA cycle module *vs.* SSI	Continuous, non-normal	Spearman rank correlation	ρ = 0.120, p = 0.12, n = 169
e	ETC module *vs.* SSI	Continuous, non-normal	Spearman rank correlation	ρ = 0.107, p = 0.16, n = 169
f	*xbp-1 vs. glr-1*	Continuous, non-normal	Spearman rank correlation	ρ = 0.182, p = 0.018, n = 169
g	*ire-1 vs. glr-1*	Continuous, non-normal	Spearman rank correlation	ρ = −0.205, p = 0.012, n = 149
h	PC2 (stress–trafficking axis) *vs.* SSI	Continuous, non-normal	Spearman rank correlation	ρ = −0.163, p = 0.034, n = 169
i	SSI *vs.* fraction variable connections	Continuous, non-normal	Spearman rank correlation	ρ = 0.072, p = 0.58, n = 63
j	SSI *vs.* fraction stable connections	Continuous, non-normal	Spearman rank correlation	ρ = 0.109, p = 0.40, n = 63
k	SSI *vs.* fraction developmental connections	Continuous, non-normal	Spearman rank correlation	ρ = −0.102, p = 0.43, n = 63

PC1, principal component 1; SSI, silent synapse index; ROS, reactive oxygen species; BH-FDR, Benjamini-Hochberg false discovery rate; TCA, tricarboxylic acid; ETC, electron transport chain; PC2, principal component 2. PC1/PC2, first and second principal components of the six metabolic gene modules; n denotes the number of neuron classes contributing to each test. Notes a–k correspond to the superscript markers in the Results text. Benjamini–Hochberg correction was applied within the family of six metabolic gene modules (note c). Note g is computed across the 149 neuron classes in which either ire-1 or glr-1 is detected. Connectome analyses (notes i–k) are restricted to the 63 neuron classes with complete transcriptomic and connectomic data.

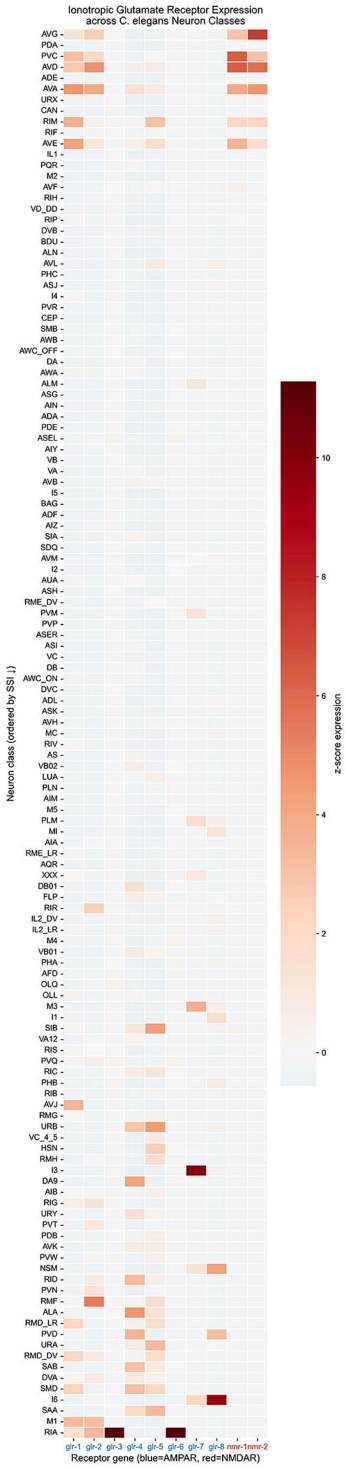

Figure 1. Ionotropic glutamate receptor expression landscape. Heatmap of z-scored expression of 10 iGluR subunits (8 AMPAR in blue labels, 2 NMDAR in red labels) across neuron classes, ordered by descending SSI. Neuron classes at the top show the highest NMDAR/AMPAR ratios.

iGluR, ionotropic glutamate receptor; AMPAR, α-amino-3-hydroxy-5-methyl-4-isoxazolepropionic acid receptor; NMDAR, N-methyl-D-aspartate receptors; SSI, Silent Synapse Index.

shown in Figure 1. All receptor genes showed high cell-type specificity ($\tau > 0.9$), with *glr-1* expression peaking in AVA interneurons and *nmr-1* in AVD (AVA and AVD are standard *C. elegans* neuron class names; both are command interneurons of the locomotor circuit). Of 169 neuron classes, 134 (79.3%) expressed only AMPA-type receptors, 23 (13.6%) were AMPAR-dominant with some NMDAR co-expression, 5 (3.0%) showed balanced expression, 1 (0.6%) was NMDAR-dominant, and 6 (3.6%) were non-glutamatergic, as shown in Figures 2a, b. No neuron class expressed only NMDARs without any AMPAR subunits, indicating that constitutively silent synapses (in the classical mammalian definition) are absent in the *C. elegans* nervous system at the transcriptomic level.

Oxidative stress burden predicts silencing propensity

Bivariate decomposition by metabolic module revealed a significant and specific association: ROS defense gene expression positively correlated with SSI ($\rho = 0.201$, $p = 0.009$; FDR-corrected $p = 0.05$). When stratified by receptor class, these metabolic profiles revealed distinct bioenergetic signatures, as shown in Figure 3a-f. While trends were observed for the composite score (Figure 3a) and for the ETC (Figure 3b), glycolysis (Figure 3c), TCA cycle (Figure 3d) and UPR (Figure 3e) modules, none of these reached significance, and autophagy showed no association; only ROS defense was significantly associated with the SSI (Figure 3f). This pattern indicates that the metabolic signal associated with silencing propensity is not bioenergetic load per se but specifically oxidative stress, the downstream consequence of mitochondrial electron transport and synaptic activity.

UPR expression as a molecular unsilencing mechanism

Individual UPR genes showed divergent associations with *glr-1* expression that are mechanistically informative, as shown in Figure 4. *ire-1*, the upstream kinase that activates XBP-1 but also mediates UPR functions unrelated to receptor trafficking, correlated negatively with *glr-1* ($\rho = -0.205$,

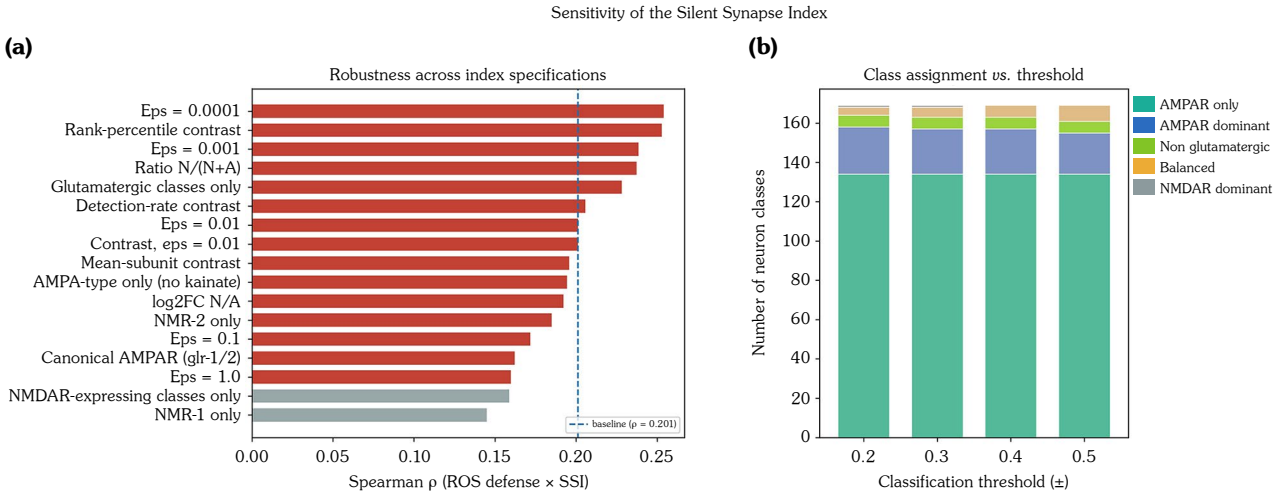

Figure 2. Sensitivity analysis of the SSI. **(a)** Robustness of the association between ROS defense and SSI across alternative index specifications. Bars represent Spearman correlation coefficients (ρ) obtained using different SSI parameterizations, receptor definitions, and analytical contrasts. The dashed vertical line indicates the baseline correlation (ρ = 0.201). **(b)** Distribution of neuron classes among SSI-based classification categories (AMPAR only, AMPAR dominant, non-glutamatergic, balanced, and NMDAR dominant) across classification thresholds ranging from ±0.2 to ±0.5. The overall distribution of neuron classes remained relatively stable across the evaluated thresholds.

SSI, Silent Synapse Index; ROS, reactive oxygen species; NMDAR, N-methyl-D-aspartate receptors; AMPAR, α-amino-3-hydroxy-5-methyl-4-isoxazolepropionic acid receptor; NMR, NMDA receptor subunit (*C. elegans* genes *nmr-1* and *nmr-2*).

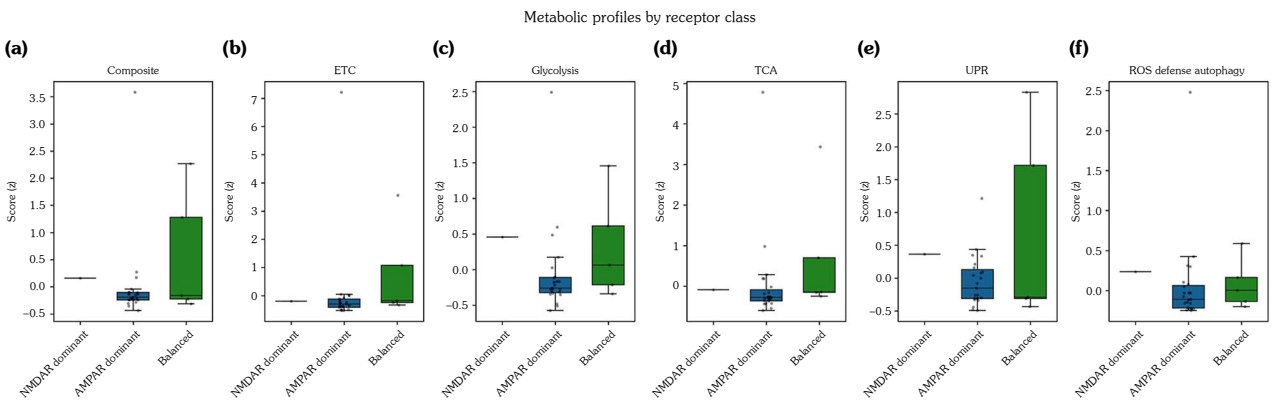

Figure 3. Metabolic module profiles by receptor class. Box plots of metabolic scores stratified by receptor class (NMDAR dominant, AMPAR dominant, balanced): **(a)** composite metabolic burden index, **(b)** mitochondrial electron transport chain, **(c)** glycolysis, **(d)** tricarboxylic acid cycle, **(e)** unfolded protein response, and **(f)** reactive oxygen species defense. Individual neuron classes are shown as points.

TCA, tricarboxylic acid; UPR, unfolded protein response; ROS, reactive oxygen species; NMDAR, N-methyl-D-aspartate receptors; AMPAR, α-amino-3-hydroxy-5-methyl-4-isoxazolepropionic acid receptor.

p = 0.012) (Figure 4a). In contrast, *xbp-1*, the downstream transcription factor that directly promotes GLR-1 export from the ER, correlated positively with *glr-1* expression across neuron classes (ρ = 0.182, p = 0.018) (Figure 4b). This divergence is consistent with the dual role of IRE-1: in neurons under ER stress, IRE-1 activation reflects protein folding burden that may compete with receptor biosynthesis, whereas XBP-1 activity specifically channels ER capacity toward AMPAR export.

Dimensionality reduction isolates oxidative stress and UPR from general metabolic load

Since metabolic pathways are highly interconnected, evaluating them in isolated bivariate correlations can obscure the true

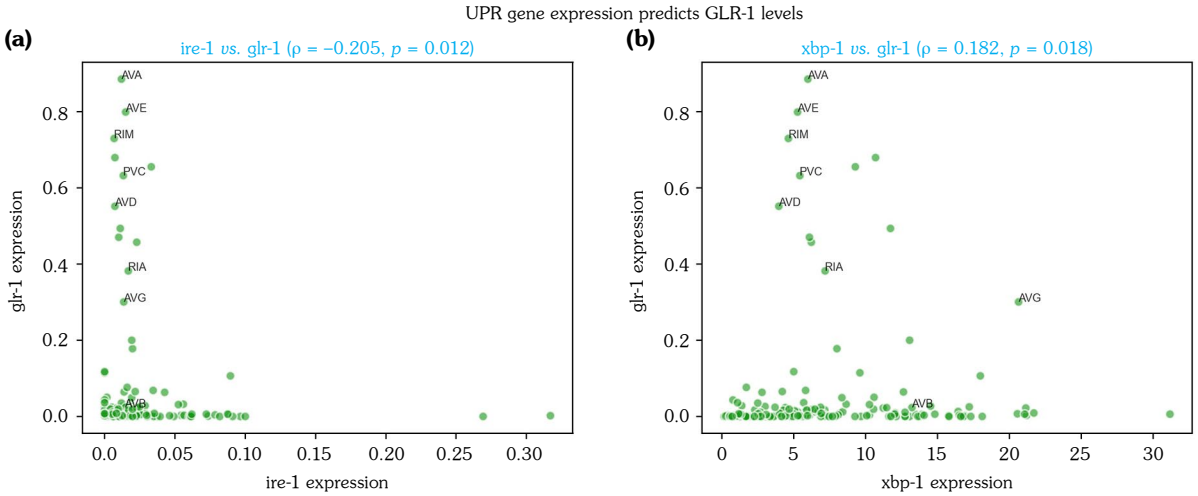

Figure 4. UPR-AMPAR trafficking axis. Scatter plots of unfolded protein response gene expression versus *glr-1* expression across neuron classes: **(a)** *ire-1* versus *glr-1* (ρ = −0.205, *p* = 0.012), **(b)** *xbp-1* versus *glr-1* (ρ = 0.182, *p* = 0.018). Note the divergent associations: *ire-1* correlates negatively with *glr-1*, reflecting its broader ER stress role, while *xbp-1* correlates positively, consistent with its specific function in promoting GLR-1 ER export. Key NMDAR-expressing neuron classes (AVA, AVD, AVG, and RIM) are labeled.

UPR, unfolded protein response; AMPAR, α-amino-3-hydroxy-5-methyl-4-isoxazolepropionic acid receptor; ER, endoplasmic reticulum; GLR-1, glutamate receptor-1; NMDAR, N-methyl-D-aspartate receptors.

AVA, AVB, AVD, AVE, AVG, PVC, RIA and RIM are standard *C. elegans* neuron class names rather than abbreviations; AVA, AVB, AVD, AVE and PVC are command interneurons of the locomotor circuit, and RIA, RIM and AVG are interneurons.

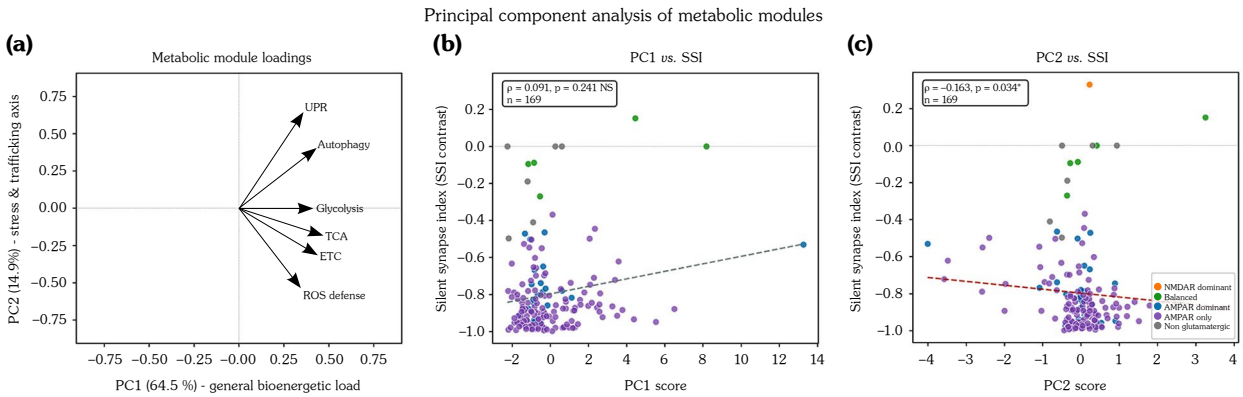

Figure 5. Dimensionality reduction reveals oxidative stress, not general bioenergetic load, drives silencing propensity. **(a)** Principal Component Analysis (PCA) biplot of the six metabolic gene modules across 169 neuron classes. Vectors indicate the loading of each module onto the first two principal components. PC1 represents "General Bioenergetic Load," with all modules contributing positively. PC2 isolates a "Stress & Trafficking Axis," characterized by an antagonism between UPR expression (positive loading) and ROS defense (negative loading). **(b)** Neuron class PC1 scores show no significant correlation with the Silent Synapse Index (SSI) (Spearman ρ = 0.091, p = 0.24), indicating total metabolic expenditure does not predict silencing. **(c)** Neuron class PC2 scores significantly and negatively correlate with SSI (Spearman ρ = −0.163, *p* = 0.034). Since ROS defense drives PC2 negatively, this confirms that higher relative oxidative stress predicts a higher proportion of silent synapses, while higher UPR capacity predicts unsilencing.

AVA, AVB, AVD, AVE, AVG, PVC, RIA and RIM are standard *Caenorhabditis elegans* neuron class names rather than abbreviations; AVA, AVB, AVD, AVE and PVC are command interneurons of the locomotor circuit, and RIA, RIM and AVG are interneurons.

biological drivers of synaptic silencing. To deconvolve these signals, we performed a PCA on the six metabolic modules across all 169 neuron classes, as shown in Figure 5. The first principal component (PC1) captured 64.5% of the variance and represented general bioenergetic load, with all six modules loading positively and uniformly

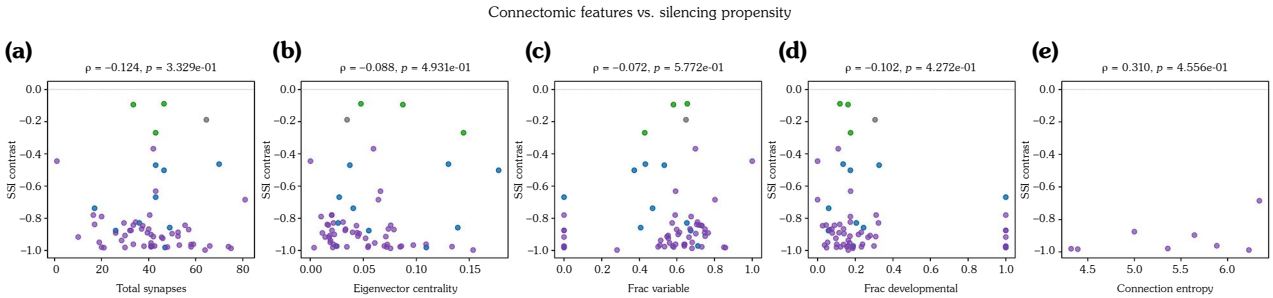

Figure 6. Connectomic features versus silencing propensity. Scatter plots of the SSI versus **(a)** total synapses, **(b)** eigenvector centrality, **(c)** fraction of variable connections, **(d)** fraction of developmental connections, and **(e)** connection entropy, for the 63 neuron classes with complete data across all modalities.

SSI, Silent Synapse Index.

(0.340 to 0.464) (Figure 5a). Crucially, PC1 did not correlate with the SSI ($\rho = 0.091$, $p = 0.241$) (Figure 5b), mathematically confirming that general metabolic expenditure alone does not predict silencing propensity.

In contrast, the second principal component (PC2, 14.9% variance) revealed a specific metabolic axis that starkly separated UPR expression (loading: +0.647) from ROS defense (loading: −0.535) and ETC expression (loading: −0.315). This specific "stress and trafficking" axis significantly predicted silencing propensity ($\rho = -0.163$, $p = 0.034$) (Figure 5c). Since PC2 is driven negatively by ROS defense and positively by UPR, this significant correlation simultaneously confirms our two independent findings: higher relative ROS burden drives synapses into a silent state, while higher UPR capacity acts as a molecular unsilencing mechanism, decreasing the NMDAR/AMPAR ratio.

Synapse stability does not predict silencing propensity

Among the 63 neuron classes with complete data across all three modalities, no significant correlations were observed between SSI and the fraction of variable, stable, or developmental connections, as shown in Figure 6a-e. Kruskal-Wallis tests comparing connectomic metrics across receptor classes were similarly non-significant. This null result is interpretable: the Witvliet classifications capture structural presence or absence of anatomical connections across individuals and developmental stages, whereas synaptic silencing operates at the functional level, a silent synapse is structurally present but functionally quiescent. The two phenomena occupy different layers of the circuit hierarchy.

DISCUSSION

We tested three predictions of synaptic silencing as a metabolic self-defense framework using the most complete nervous system transcriptomic-connectomic dataset available in any organism. Two of the three predictions received partial or full support, and the pattern of results refines the original framework in a mechanistically informative direction.

The central finding that oxidative stress defense gene expression, but not total metabolic load, predicts silencing propensity, sharpens the metabolic self-defense hypothesis.

Reactive oxygen species are a direct byproduct of mitochondrial respiration and are elevated by sustained synaptic activity.[15,16] Neurons with higher constitutive ROS defense investment are, by implication, neurons that chronically experience greater oxidative stress, and these are the neurons that maintain a higher NMDAR/AMPAR ratio. Silencing may thus be better understood not as an energy-saving measure per se, but as an oxidative damage mitigation strategy: reducing the number of active excitatory synapses reduces the demand for mitochondrial adenosine triphosphate production, which in turn reduces ROS generation. The metabolic self-defense is specifically a defense against oxidative harm.

Our dimensionality reduction (PCA) further clarified this by separating general bioenergetic load from specific cellular stress responses. While the primary metabolic component (PC1) showed no relationship with silencing, the stress and trafficking axis (PC2) significantly predicted the NMDAR/AMPAR ratio. The antagonistic loadings of UPR and ROS defense on this axis are consistent with established molecular biology. In *C. elegans*, *ire-1* and *xbp-1* mutations prevent GLR-1 export from the ER,[11] and GLR-1 trafficking to synapses is required for long-term memory.[17] Our single-gene data reveal this nuance: *xbp-1* expression positively correlates with *glr-1* levels, consistent with its direct role in promoting AMPAR ER export, while *ire-1* expression correlates negatively with *glr-1*, reflecting its broader role in ER stress signaling that competes with receptor biosynthesis. The UPR, particularly its XBP-1 effector arm, is thus interpretable as the molecular machinery for synapse unsilencing: the process by which silent synapses are converted to active ones through AMPAR insertion, precisely as described in the mammalian long-term potentiation literature.[4,18]

The absence of constitutively silent (NMDAR-only) neuron classes in *C. elegans* is notable. Every neuron class expressing NMDARs also expresses at least some AMPAR subunits, albeit at varying ratios. This divergence from the mammalian binary silent/active distinction is biophysically consistent with the graded, non-spiking nature of *C. elegans* neurotransmission. In a spiking mammalian neuron, the rapid, massive depolarization of an action potential is sufficient to relieve the voltage-dependent Mg2+ block of the NMDAR. In contrast, the isopotential, analog voltage shifts in *C. elegans* require a baseline AMPAR conductance to continuously tune the postsynaptic membrane potential and dynamically regulate Mg2+ relief. Complete AMPAR withdrawal in this analog regime would sever the voltage transfer function entirely, rendering the NMDAR permanently inaccessible.

Therefore, rather than a binary switch, the worm appears to utilize a continuous spectrum of NMDAR/AMPAR ratios, a "graded silencing" strategy that continuously calibrates metabolic cost against synaptic gain.

Methodological considerations: Transcriptomic propensity and the proteomic bottleneck

While the CeNGEN atlas provides unprecedented single-neuron resolution, it is inherently limited by the transcriptome-to-proteome gap: steady-state messenger ribonucleic acid (mRNA) levels of NMDAR and AMPAR subunits represent a cell's biosynthetic investment rather than its instantaneous synaptic physiology, as they do not capture post-translational modifications or dynamic membrane insertion. However, this limitation is mitigated by two factors in our analysis. First, unlike highly arborized mammalian pyramidal cells where somatic transcription is heavily decoupled from synaptic proteomes, the compact, often unipolar or bipolar neuroanatomy of *C. elegans* facilitates a tighter spatial and biochemical coupling between global transcriptional programs and local synaptic states. Second, and most critically, our finding that the UPR*/xbp-1* axis significantly covaries with the SSI directly addresses the proteomic bottleneck. The ER folding and export machinery is the primary rate-limiting step between receptor transcription and functional synaptic deployment.[11] The tight integration of oxidative stress defense, UPR capacity, and receptor mRNA ratios strongly suggests that the transcriptomic SSI reflects an actively managed, cell-wide bioenergetic strategy rather than uncoupled transcriptional noise.

Several other limitations warrant mention. First, the SSI as computed here reflects the steady-state NMDAR/AMPAR ratio across a neuron class, not synapse-specific silencing. Second, while the merged dataset required for connectomic integration ($n = 63$ neuron classes) is the most comprehensive available, its statistical power is mathematically bounded. A post-hoc power analysis indicates that a sample size of 63 provides 80% power to detect a true correlation of $\rho \geq 0.35$ at $\alpha = 0.05$. Therefore, while we can confidently exclude large structural drivers of silencing, we cannot definitively rule out the existence of small-to-moderate structural effects ($\rho < 0.35$). Third, *C. elegans* neurons use graded potentials without sodium-based action potentials, making the Mg2+ voltage-gating mechanism that defines mammalian silent synapses functionally different in this organism.

In conclusion, the *C. elegans* nervous system provides initial cross-species support for synaptic silencing as a metabolic self-defense framework, with a key refinement: the metabolic signal most closely associated with silencing propensity is oxidative stress rather than total bioenergetic load. The UPR-AMPAR trafficking axis functions as a conserved unsilencing mechanism across nematodes and mammals. These findings establish the integration of CeNGEN with connectome data as a tractable platform for testing predictions of metabolic-synaptic coupling theories with single-neuron resolution. Future experimental work, particularly examining GLR-1 trafficking dynamics in ROS-stressed neurons using fluorescent reporter strains, will be essential to determine whether the transcriptomic associations identified here reflect causal mechanisms.

Data Sharing Statement: All data analyzed in this study are publicly available: the CeNGEN single-cell RNA-sequencing dataset via the WormBase-curated AnnData archive (data.caltech.edu/records/qaqhb-r9m40) and the developmental connectome via the supplementary tables of Witvliet et al.[9] Derived data tables are available from the corresponding author upon reasonable request.

Author Contributions: C.T., B.T.: Idea/concept, design, analysis and/or interpretation, literature review, writing the article, critical review, references, materials; B.T.: Control/supervision, data collection and/or processing.

Conflict of Interest: The authors declared no conflicts of interest with respect to the authorship and/or publication of this article.

Funding: The authors received no financial support for the research and/or authorship of this article.

Acknowledgments: We thank the CeNGEN consortium and Daniel Witvliet for making their datasets publicly available, and WormBase for curating *C. elegans* single-cell data in standardised formats.

AI Disclosure: The authors declare that artificial intelligence (AI) tools were not used, or were used solely for language editing, and had no role in data analysis, interpretation, or the formulation of conclusions. All scientific content, data interpretation, and conclusions are the sole responsibility of the authors. The authors further confirm that AI tools were not used to generate, fabricate, or 'hallucinate' references, and that all references have been carefully verified for accuracy.

REFERENCES

1. Attwell D, Laughlin SB. An energy budget for signaling in the grey matter of the brain. J Cereb Blood Flow Metab 2001;21:1133-45. doi: 10.1097/00004647-200110000-00001.
2. Harris JJ, Jolivet R, Attwell D. Synaptic energy use and supply. Neuron 2012;75:762-77. doi: 10.1016/j.neuron.2012.08.019.
3. Topcular B, Turkmen C. Synaptic silencing as metabolic self-defence: From energy crisis to connectivity collapse in Alzheimer's Disease. Zenodo; 2026. doi: 10.5281/zenodo.19329122.
4. Kerchner GA, Nicoll RA. Silent synapses and the emergence of a postsynaptic mechanism for LTP. Nat Rev Neurosci 2008;9:813-25. doi: 10.1038/nrn2501.
5. Motta A, Berning M, Boergens KM, Staffler B, Beining M, Loomba S, et al. Dense connectomic reconstruction in layer 4 of the somatosensory cortex. Science 2019;366:eaay3134. doi: 10.1126/science.aay3134.
6. Yellen G. Fueling thought: Management of glycolysis and oxidative phosphorylation in neuronal metabolism. J Cell Biol 2018;217:2235-46. doi: 10.1083/jcb.201803152.
7. White JG, Southgate E, Thomson JN, Brenner S. The structure of the nervous system of the nematode Caenorhabditis elegans. Philos Trans R Soc Lond B Biol Sci 1986;314:1-340. doi: 10.1098/rstb.1986.0056.
8. Cook SJ, Jarrell TA, Brittin CA, Wang Y, Bloniarz AE, Yakovlev MA, et al. Whole-animal connectomes of both Caenorhabditis elegans sexes. Nature 2019;571:63-71. doi: 10.1038/s41586-019-1352-7.
9. Witvliet D, Mulcahy B, Mitchell JK, Meirovitch Y, Berger DR, Wu Y, et al. Connectomes across development reveal principles of brain maturation. Nature 2021;596:257-61. doi: 10.1038/s41586-021-03778-8.
10. Taylor SR, Santpere G, Weinreb A, Barrett A, Reilly MB, Xu C, et al. Molecular topography of an entire nervous system. Cell 2021;184:4329-47.e23. doi: 10.1016/j.cell.2021.06.023.
11. Shim J, Umemura T, Nothstein E, Rongo C. The unfolded protein response regulates glutamate receptor export from the endoplasmic reticulum. Mol Biol Cell 2004;15:4818-28. doi: 10.1091/mbc.e04-02-0108.
12. Brockie PJ, Maricq AV. Ionotropic glutamate receptors: Genetics, behavior and electrophysiology. WormBook 2006:1-16. doi: 10.1895/wormbook.1.61.1.
13. da Veiga Beltrame E. CeNGEN scRNAseq dataset wrangled into standard WormBase anndata – 100k C. elegans cells FACS sorted for neurons in L4 larvae. (Version 1.0) [Dataset]. CaltechDATA; 2021. Available from: https://data.caltech.edu/records/qaqhb-r9m40. [Accessed: January 15, 2026].

14. Yanai I, Benjamin H, Shmoish M, Chalifa-Caspi V, Shklar M, Ophir R, et al. Genome-wide midrange transcription profiles reveal expression level relationships in human tissue specification. Bioinformatics 2005;21:650-9. doi: 10.1093/bioinformatics/bti042.
15. Bindokas VP, Jordán J, Lee CC, Miller RJ. Superoxide production in rat hippocampal neurons: Selective imaging with hydroethidine. J Neurosci 1996;16:1324-36. doi: 10.1523/JNEUROSCI.16-04-01324.1996.
16. Brennan AM, Suh SW, Won SJ, Narasimhan P, Kauppinen TM, Lee H, et al. NADPH oxidase is the primary source of superoxide induced by NMDA receptor activation. Nat Neurosci 2009;12:857-63. doi: 10.1038/nn.2334.
17. Rose JK, Kaun KR, Chen SH, Rankin CH. GLR-1, a non-NMDA glutamate receptor homolog, is critical for long-term memory in Caenorhabditis elegans. J Neurosci 2003;23:9595-9. doi: 10.1523/JNEUROSCI.23-29-09595.2003.
18. Malenka RC, Nicoll RA. Long-term potentiation--a decade of progress? Science 1999;285:1870-4. doi: 10.1126/science.285.5435.1870.